Manipulating shear-induced non-equilibrium transitions by feedback control

Tarlan A. Vezirov[1], Sascha Gerloff[1] and Sabine H. L. Klapp[1]

[1] *Institut für Theoretische Physik, Hardenbergstr. 36, Technische Universität Berlin, D-10623 Berlin, Germany*

arXiv:1403.6994v1 [cond-mat.soft] 27 Mar 2014

PACS 05.70.Ln – Nonequilibrium and irreversible thermodynamics
PACS 87.19.lr – Control theory and feedback
PACS 82.70.Dd – Colloids

Abstract – Using Brownian Dynamics (BD) simulations we investigate non-equilibrium transitions of sheared colloidal films under controlled shear stress σ_{xz}. In our approach the shear rate $\dot{\gamma}$ is a dynamical variable, which relaxes on a timescale τ_c such that the instantaneous, configuration-dependent stress $\sigma_{xz}(t)$ approaches a pre-imposed value. Investigating the dynamics under this "feedback-control" scheme we find unique behavior in regions where the constitutive curve $\sigma_{xz}(\dot{\gamma})$ of the uncontrolled system is monotonic. However, in non-monotonic regions our method allows to *select* between dynamical states characterized by different in-plane structure and viscosities. Indeed, the final state strongly depends on τ_c relative to an *intrinsic* relaxation time of the uncontrolled system. The critical values of τ_c are estimated on the basis of a simple model.

Introduction. – Soft matter under shear flow can display rich nonlinear behaviour involving transitions between different dynamical states [1,2], spontaneous spatial symmetry-breaking [3] and shear banding [4–8], heterogeneous local dynamics [9, 10], and (rheo-)chaos [11–13]. These intriguing phenomena often strongly affect the *rheological* properties of the system. Understanding shear-induced effects in, e.g, complex surfactant solutions [14] or liquid crystals [1], colloids [15–17], soft glasses [9, 10, 18], and active fluids [19], is thus a major current topic connecting non-equilibrium physics and soft material science.

A quantity of particular interest is the flow curve (or constitutive) curve [8, 20], that is, the shear stress σ as function of the shear rate $\dot{\gamma}$, both of which can serve as experimental control parameters. In many examples, the curve $\sigma(\dot{\gamma})$ behaves not only nonlinear (indicating shear-thinning [21,22], shear-thickening [22,23], sometimes connected irregular (chaotic) rheological response [13, 24]), but becomes also multivalued, i.e. different shear rates lead to the same stress. In complex fluids of e.g. wormlike micelles, this multivalued property is in fact, a universal indicator of a *shear-banding* instability, i.e. a separation of the (formerly homogeneous) system into coexisting bands characterized by a smaller and a larger local shear rate [20]. In soft (colloidal) glasses, multivalued functions $\sigma(\dot{\gamma})$ occur as transient phenomena after a sudden switch-on of shear stress (Bauschinger effect) [25], or in the vicinity of the so-called yield stress [26]; in these systems one observes strong dynamical heterogeneities [10]. A further intriguing feature is that close to such nonmonotonicities, the system's behaviour strongly depends on whether one uses the shear stress or the shear rate as a control parameter [12,27] (in fact, both choices are common in rheological experiments [18, 28, 29]).

Here we present BD computer simulation results of yet another system with multivalued stress-strain curve, that is, a thin colloidal film sheared from an (equilibrium) state within in-plane crystalline order in a planar Couette geometry. In this films, the non-monotonicity arises due to successive non-equilibrium transitions from elastic over molten into reentrant frozen states [17,30]. Our focal point is to explore such nonlinear systems in presence of controlled *shear stress*. In fact, so far most simulations of sheared colloids have been done under fixed shear rate $\dot{\gamma}$, exceptions being e.g. Refs. [10, 26, 31], where constant σ has been realized by fixing the force acting on the atoms forming the walls. Here we introduce an alternative, easy-to-apply scheme to control σ which has been previously used by us in continuum approaches of sheared liquid crystals [27]. In that scheme $\dot{\gamma}$ (which directly enters the BD equations of motion) becomes a dynamical variable whose time dependence is governed by a relaxation equation involving a time scale τ_c. The relaxation is based on the difference between the instantaneous (configuration-

dependent) stress $\sigma(t)$ and a preimposed value σ_0. The idea of adapting $\dot\gamma$ is inspired by experimental of stress-controlled systems [29]. Our scheme differs from earlier schemes [10, 26, 31] where the desired value σ_0 is imposed *instantaneously*. Moreover, due to the coupling to the particle positions our method corresponds to a "feedback" (closed-loop) control scheme, which is similar in spirit to e.g. a Berendsen thermostat for temperature control [32]. However, here the choice for τ_c is found to be crucial for the observed dynamical behaviour. In particular we demonstrate that, if our scheme is applied within the multivalued regime of $\sigma(\dot\gamma)$, the final state strongly depends on the magnitude of τ_c relative to important intrinsic time scales of the system. Thus, the stress-control can be used to deliberately *select* a desired dynamical state.

Model and simulation details. – We consider a model colloidal suspension where two particles with distance r_{ij} interact via a combination of a repulsive Yukawa potential, $u_{\rm Yuk}(r_{ij}) = W \exp\left[-\kappa r_{ij}\right]/r_{ij}$ and a repulsive soft-sphere potential $u_{\rm SS}(r_{ij}) = 4\epsilon_{\rm SS}(d/r_{ij})^{12}$ involving the particle diameter d [17]. The interaction parameters are set in accordance to a real suspension of charged silica macroions (for details, see [33,34]). Specifically, at the density considered (see below), the interaction strength $W/(k_{\rm B}Td) \approx 123$ (where $k_{\rm B}T$ the thermal energy) and the inverse screening length $\kappa \approx 3.0d^{-3}$. Spatial confinement is modeled by two plane parallel, smooth, uncharged surfaces separated by a distance $L_{\rm z}$ along the z direction and of infinite extent in the x–y plane. We employ a purely repulsive fluid-wall decaying as z^{-9}. Our investigations are based on standard BD simulations, where the position of particle i is advanced according to [35]

$$\mathbf{r}_i(t+\delta t) = \mathbf{r}_i(t) + \frac{D_0}{k_B T}\mathbf{F}_i(t)\delta t + \delta\mathbf{W}_i + \dot\gamma z_i(t)\delta t \mathbf{e}_x, \quad (1)$$

where $\mathbf{F}_i$ is the total conservative force acting on particle i, D_0 is the short-time diffusion constant, and $\delta\mathbf{W}_i$ is a random displacement with white-noise properties. We impose a linear shear profile [see last term in eq. (1)] representing flow in x- and gradient in z-direction, characterized by uniform shear rate $\dot\gamma$. This approximation has also been employed in other recent simulation studies of sheared colloids [15, 36]; the same holds for the fact that we neglect hydrodynamic interactions.

One quantity of prime interest in our study is the x-z component of the stress tensor,

$$\sigma_{\rm xz} = \left\langle \frac{1}{V}\sum_i \sum_{j>i} F_{x,ij} z_{ij} \right\rangle. \quad (2)$$

Thus, we consider only the configuration-dependent contribution to $\sigma_{\rm xz}$; the kinematic contribution (which involves the velocity components in x- and z-direction) is negligible under the highly confined conditions here.

Based on the shear stress, we introduce a feedback scheme as follows. Starting from an initial value for $\dot\gamma$ we calculate, in each time step, the configuration-dependent stress $\sigma_{\rm xz}$ from eq. (2) and adjust $\dot\gamma$ via the relaxation equation

$$\frac{d}{dt}\dot\gamma = \frac{1}{\tau_c}\frac{\sigma_0 - \sigma_{\rm xz}(t)}{\eta_0}, \quad (3)$$

where σ_0 is a *pre-imposed* value of $\sigma_{\rm xz}$, and τ_c determines the time scale of relaxation. Also, η_0 is the shear viscosity obtained for $\dot\gamma \to 0$ (linear-response regime). Through eq. (3), $\dot\gamma$ becomes an additional dynamical variable. Therefore, and since $\sigma_{\rm xy}(t)$ depends on the instantaneous configuration $\{\mathbf{r}_i(t)\}$ of the particles, simultaneous solution of the $N+1$ equations of motion (1) and (3) forms a closed feedback loop with *global* coupling.

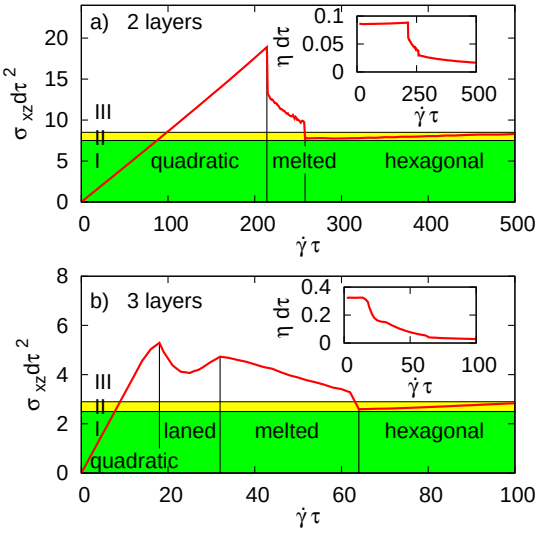

Fig. 1: (Color online) Shear stress and shear viscosity (insets) for bi- and trilayer systems as function of the applied strain. Regions indicated as I, II, III are discussed in the main text.

We focus on systems at high density, specifically $\rho d^3 = 0.85$, and strong confinement, $L_{\rm z} = 2.2d$. The corresponding equilibrium system forms a colloidal bilayer with crystalline in-plane structure [34]. We also show some data with $L_{\rm z} = 3.2d$, yielding three layers. The values $L_{\rm z} = 2.2$ and 3.2 have been chosen because the equilibrium lattice structure is quadratic [34] (other values would lead to hexagonal equilibrium structures which do not show the shear-induced transitions discussed here). Periodic boundary conditions were applied in flow (x) and vorticity (y) direction. The number of particles was $N = 1058$ and 1587 for $L_{\rm z} = 2.2d$ and $3.2d$, respectively. The timestep was set to $\delta t = 10^{-5}\tau$ where $\tau = d^2/D_0$ the time unit.

Shear-induced transitions. – We start by considering flow curves for systems at constant $\dot\gamma$. The functions $\sigma_{\rm xz}(\dot\gamma)$ for both, two- and three layer systems are plotted in fig. 1, where we have included data for the viscosities $\eta = \sigma_{\rm xz}/\dot\gamma$. Both systems are clearly characterized by a nonmonotonic flow curve, accompanied by pronounced shear-thinning. At small shear rates, the systems display linear stress, related to an elastic response of the quadratic

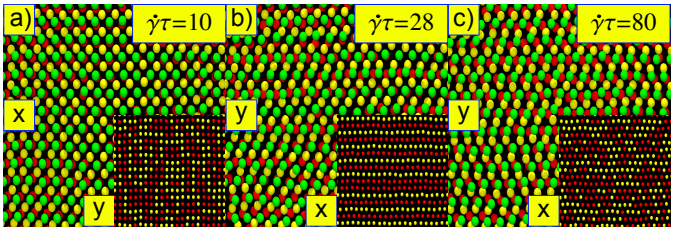

Fig. 2: (Color online) Snapshots of a colloidal trilayer at three different shear rates corresponding to a) quadratic, b) laned, and c) hexagonal state. In the main figures, the three colours correspond to particles in the three layers. In the insets, the two colours indicate particles moving in the region $z > 0$ and $z < 0$, where $z = 0$ is the middle plane of the confined system.

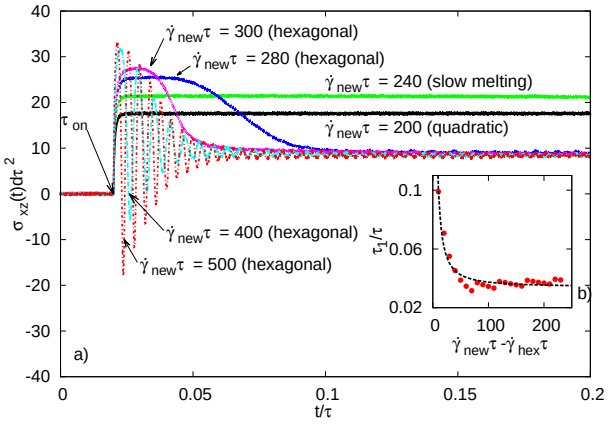

Fig. 3: (Color online) Response of $\sigma_{xz}(t)$ to a sudden switch-on (at time τ_{on}) of shear with different rates $\dot\gamma_{new}\tau$, starting from the equilibrium (quadratic) state. The inset shows the fit of the relaxation times τ_1 according to eq. (4).

in-plane lattice structure. An exemplary simulation snapshot for the three-layer system is shown in fig. 2a) (see Ref. [17] for corresponding results for the bilayer). In fact, within the elastic regime the layer velocities are zero, i.e., the particles are "locked". Further increase of the shear rate then destroys the quadratic order, as indicated by the sudden decrease of σ_{xz} (onset of shear-thinning). The bilayer system here enters directly a shear-molten state, accompanied by an increase of the layer velocity from zero to finite values [17]. At the same time, the slope of the flow curve becomes negative, meaning that the system is mechanically unstable [37]. Somewhat different behaviour is found in the trilayer system which displays, before melting, an intermediate state [see fig. 2b)]: This state is characterized by a non-zero layer velocity. In addition, the middle layer separates into two sublayers, in which the particles are ordered in "lanes" (see inset of fig. 2b) and move with the velocity of the corresponding outer layer (a more detailed discussion of this "laned" state will be given elsewhere [38]). Only further increase of $\dot\gamma$ then yields a shear-molten state characterized by a decreasing flow curve (in analogy to the bilayer). Finally, both systems transform into a state with in-plane hexagonal ordering [see fig. 2c)] and low viscosity. As demonstrated earlier by us [17] the mechanism of relative motion involves collective oscillations of the particles around lattice sites, consistent with recent experiments of 3D sheared colloidal crystals [16]. Regarding the stress, we see that the hexagonal regime is (in both systems) characterized by a slight increase of σ_{xz} with $\dot\gamma$. As a consequence, there is a parameter range (indicated as region "II" in fig. 1) where the flow curve is *multivalued*, that is, different $\dot\gamma$ lead to the same σ_{xz}.

Intrinsic time scales. – Before exploring the impact of shear-stress control, which involves a time scale itself through the parameter τ_c [see eq. (3)], we take a closer look at the *intrinsic* time scales characterizing the uncontrolled systems. We focus on the bilayer (the same findings apply qualitatively on the trilayer) and consider the response of the unsheared equilibrium system, which is in a quadratic state, to a *sudden* switch-on at time τ_{on} of shear with rate $\dot\gamma_{new}$. The resulting time dependence of the instantaneous stress is plotted in fig. 3. If $\dot\gamma_{new}\tau$ has a value pertaining to the quadratic or shear-molten state, the shear stress jumps at τ_{on} to non-zero values but then settles quickly to its steady-state value [see fig. 1]. The overall behaviour of $\sigma_{xz}(t)$ is monotonic. On the contrary, for shear rates related to the hexagonal steady state ($\dot\gamma_{new}\tau > \dot\gamma_{hex}\tau \approx 260$), we observe a well-pronounced stress overshoot, similar to what is observed in soft glassy systems [25]. Related to this feature, the relaxation time τ_1 which the stress needs to approach its steady-state value becomes quite large, in fact, $\tau_1/\tau = \mathcal{O}(10^{-2})$. Closer inspection shows that the actual value of τ_1 as well as the functional behavior of $\sigma_{xz}(t)$ strongly depends on the distance between $\dot\gamma_{new}\tau$ and the threshold between shear-molten and hexagonal state, $\dot\gamma_{hex}\tau$: the smaller this distance is, the larger becomes τ_1, and the more sensitive it is against small changes of the shear rate. Moreover, a sudden quench *deep* into the hexagonal state leads to an *oscillatory* relaxation of the stress $\sigma_{xz}(t)$ [see curves $\dot\gamma_{new}\tau = 400, 500$], with τ_1 (which now corresponds to the relaxation time of the envelope) being still quite large. Taken together, for $\dot\gamma_{new}\tau > \dot\gamma_{hex}\tau$, τ_1 can be fitted according to (see inset in fig. 3)

$$\tau_1 = \frac{a}{(\dot\gamma_{new}\tau - \dot\gamma_{hex}\tau)^b} + c, \qquad (4)$$

where we find $a/\tau = 1.356$, $b = 1.3$, and $c/\tau = 0.034$ (setting $\dot\gamma_{hex}\tau = 260$). The oscillations occurring at large $\dot\gamma_{new}$ induce yet a different time scale τ_2, which is smaller than τ_1. Specifically, we find $\tau_2/\tau = \mathcal{O}(10^{-3})$. The physical reason for these oscillations is the "zig-zag" motion of particles in adjacent layers [17]. This motion is accompanied by periodic variations of nearest-neighbor distances, and thus, pair forces, which eventually leads to oscillations of $\sigma_{xz}(t)$.

For comparison we have also investigated the reverse

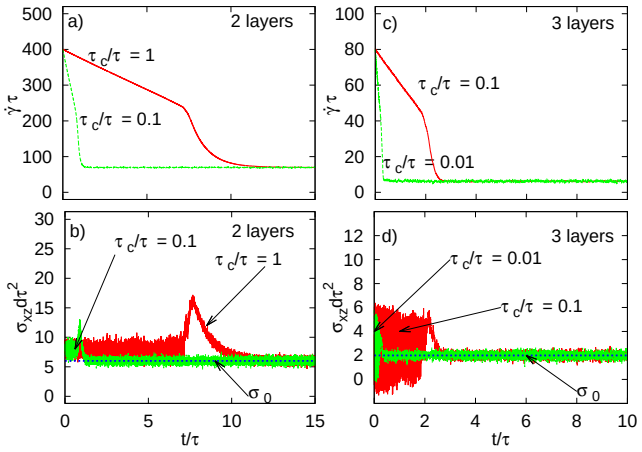

Fig. 4: (Color online) Time dependence of the instantaneous shear rate and shear stress for a bilayer- [a), b)] and a trilayer system [c), d)] in presence of feedback control within region I. The imposed stress was set to $\sigma_0 d\tau^2 = 6(2)$ for the bilayer (trilayer) system. Various values of τ_c/τ are considered.

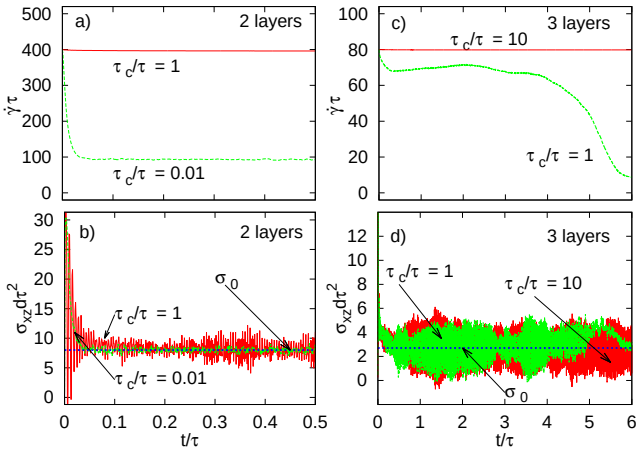

Fig. 5: (Color online) Same as fig. 4, but for $\sigma_0 d\tau^2 = 8(2.7)$ for the bilayer (trilayer) system (region II).

situation, where the system is initially in a hexagonal steady state at shear rate $\dot{\gamma}_{\rm init}$. We then switch off the shear and consider the relaxation towards the quadratic equilibrium state. Quite independently of $\dot{\gamma}_{\rm init}$, this relaxation is monotonic and characterized by a very short time, $\tau_3/\tau = \mathcal{O}(10^{-4})$.

Impact of feedback control. – We now discuss the impact of our shear stress control scheme defined in eq. (3). The latter involves the zero-shear viscosity, η_0, which is estimated from fig. 1 to $\eta_0 = 0.086/d\tau$ and $0.323/d\tau$ for the bilayer and trilayer, respectively.

The overall dynamical behaviour under feedback control strongly depends on the value of σ_0 (imposed shear) relative to the flow curve of the original system (see fig. 1). We can differentiate between regimes I, II, and III, which are indicated in fig. 1.

For a σ_0 chosen in region I, the response of the system is *unique*, that is, the final state is independent of the control timescale τ_c, as well as of the initial shear rate $\dot{\gamma}_{\rm init}$ and the initial microstructure. As an "extreme" example demonstrating this injectivity, we plot in fig. 4a)-b) the functions $\dot{\gamma}(t)$ and $\sigma_{\rm xz}(t)$ for the bilayer system at $\sigma_0 d\tau^2 = 6$ and various τ_c, starting from a *hexagonal* configuration (and $\dot{\gamma}_{\rm init}\tau = 400$). In all cases, the shear rate decreases towards the value $\dot{\gamma}\tau \approx 70$ and the structure relaxes into the quadratic state pertaining to the value $\sigma_{\rm xz} d\tau^2 = 6$ in the *uncontrolled* system. This indicates that the quadratic state in region I is indeed the only fixed point of the dynamics. We also see from fig. 4a) that the relaxation time into this steady state increases with τ_c. Figure 4b) additionally shows that $\sigma_{\rm xz}(t)$ displays a pronounced peak at a time close towards the end of the relaxation regime. This peak indicates the time after which the initial hexagonal transforms into quadratic ordering. Similar behaviour occurs in region I of the trilayer system [see fig. 4c)-d)] where, however, fluctuations of $\sigma_{\rm xz}(t)$ are generally larger.

We now choose σ_0 within region II of the flow curve, where there are three different shear rates (and thus, three fixed points) pertaining to the same stress (see fig. 1). We focus on systems which are initially in a quadratic configurations, whereas the initial shear rate $\dot{\gamma}_{\rm init}$ has a value pertaining to the hexagonal state (other initial conditions will be discussed below). The impact of τ_c on the time dependence of $\dot{\gamma}(t)$ and $\sigma_{\rm xz}(t)$ is shown in fig. 5. For small values of the control timescale the systems stays in the initial lattice configuration, i.e., $\dot{\gamma}$ relaxes towards the value pertaining to the quadratic state ($\dot{\gamma}\tau \approx 90$). Different behaviour occurs at larger values of τ_c/τ: Although the initial structure is quadratic, the final state is *hexagonal*, and the shear rate essentially remains at its high initial value. We stress that these findings crucially depend on the choice of $\dot{\gamma}_{\rm init}$. In particular, the dependency of the long-time behaviour on τ_c/τ only arises for large values of $\dot{\gamma}_{\rm init}$; for small values the system remains in the quadratic state irrespective of τ_c. An overview of the final dynamical states in the feedback-controlled bilayer at $\sigma_0 d\tau^2 = 8$ and various combinations of $\dot{\gamma}_{\rm init}$ and τ_c/τ (assuming a quadratic initial structure) is given in fig. 6. The colour code indicates the ratio of local bond-order parameters $\langle \Psi_6/\Psi_4 \rangle$ (for a definition of the Ψ_n see, e.g., Ref. [17]). The restriction to values $\langle \Psi_6/\Psi_4 \rangle \leq 6$ is related to the actual values observed in the simulations. From fig. 6 one clearly sees that for initial shear rates $\dot{\gamma}_{\rm init}\tau > \dot{\gamma}_{\rm hex}\tau \approx 260$, the final state of the feedback-controlled system depends on τ_c/τ. This is in contrast to the uncontrolled system which becomes hexagonal for all $\dot{\gamma}_{\rm init} > \dot{\gamma}_{\rm hex}$. For a hexagonal initial configuration the diagram (not shown here) looks similar from a qualitative point of view; however, the range of control times where the system retains a hexagonal state despite of $\dot{\gamma}_{\rm init} < \dot{\gamma}_{\rm quad}$ (with $\dot{\gamma}_{\rm quad}$ being the threshold between quadratic/melted states) is much smaller.

We conclude that, by varying τ_c and the initial structure, we can "switch" between the two stable, steady-state

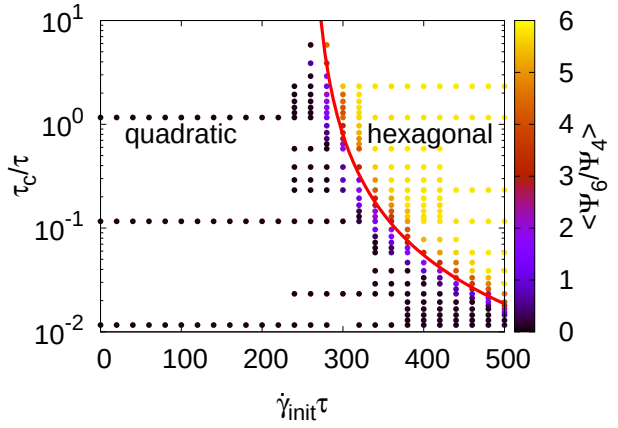

Fig. 6: (Color online) State diagram indicating long-time lattice structures. All simulations were started from a quadratic initial structure. The line shows the result from eq. (8).

configurations arising in the multivalued region of the uncontrolled system. Indeed, the dynamics under feedback control *never* evolves towards the intermediate, shear-molten states, consistent with the fact that that these states are mechanically unstable. This holds also in region III of the flow curve of the uncontrolled system, e.g., for $\sigma_0 d\tau^2 = 16(5)$ for the bilayer (trilayer): Here, a small value of τ_c yields relaxation towards the quadratic state, whereas for large τ_c, the system very slowly evolves into a hexagonal state. However, within the time scale of our simulations we did not reach the corresponding (very high) shear rates. Finally, we note that completely analogous behaviour is found in the trilayer system [see fig. 5b)-c)] for a σ_0 pertaining to the regime where quadratic, melted and hexagonal states exist.

Transition line. – The most significant observation from fig. 6 is that at high values of $\dot{\gamma}_{\rm init}$, the feedback-controlled system can achieve *either* the hexagonal or the quadratic configuration, provided that we start from a quadratic configuration and choose τ_c/τ accordingly. We now propose a simple model which allows us to estimate the *transition* values of the control time, $\tau_c^{\rm trans}$.

The physical idea behind our model is that, with the initial conditions described above, relaxation into the hexagonal state only occurs if the *reorganization* time $\tau_{\rm reorg}$ required by the system to transform from a quadratic into a hexagonal configuration, is smaller than the time $\tau_{\rm decay}$ in which $\dot{\gamma}$ decays to a value pertaining to the quadratic state. We can estimate $\tau_{\rm decay}$ from eq. (3) if we assume, for simplicity, a *linear* relationship $\sigma_{\rm xz}(t) = m\dot{\gamma}(t)$ (note that such a relationship is indeed nearly fulfilled *within* the quadratic and hexagonal states, see fig. 1). Under this assumption eq. (3) can be easily solved, yielding (with $m = \eta_0$)

$$\dot{\gamma}(t) = \eta_0^{-1} e^{-t/\tau_c} \left(\eta_0 \dot{\gamma}_{\rm init} - \sigma_0 + e^{t/\tau_c} \sigma_0 \right). \qquad (5)$$

From eq. (5) we find that the decay time of $\dot{\gamma}$ to the threshold value $\dot{\gamma}_{\rm hex}$ (below which the hexagonal state of the uncontrolled system is unstable) is given by

$$\tau_{\rm decay} = \tau_c \ln \left(\frac{\eta_0 \dot{\gamma}_{\rm init} - \sigma_0}{\eta_0 \dot{\gamma}_{\rm hex} - \sigma_0} \right). \qquad (6)$$

To estimate the reorganization time $\tau_{\rm reorg}$ (from the initial quadratic into a hexagonal configuration), we assume that its dependence on $\dot{\gamma}_{\rm init}$ is analogous to that of the relaxation time τ_1 introduced for the *uncontrolled* system [see eq. (4)]. Specifically, we make the ansatz

$$\tau_{\rm reorg} = \frac{a'}{(\dot{\gamma}_{\rm init}\tau - \dot{\gamma}_{\rm hex}\tau)^{1.3}}. \qquad (7)$$

Thus, we take the same exponent b as in the uncontrolled system [see eq. (4)]. As stated above, a crucial assumption of our model is that the system can only reach the hexagonal state if $\tau_{\rm reorg}$ does not exceed $\tau_{\rm decay}$. Note that the latter involves (in fact, is proportional to) the time τ_c. By equating expressions (6) and (7) for $\tau_{\rm decay}$ and $\tau_{\rm reorg}$, respectively, we can therefore find an expression for the *minimal* control time, $\tau_c^{\rm trans}$, above which the system reaches the hexagonal state, that is

$$\tau_c^{\rm trans} = \frac{a'}{(\dot{\gamma}_{\rm init}\tau - \dot{\gamma}_{\rm hex}\tau)^b \ln\left(\frac{\eta_0\dot{\gamma}_{\rm init}-\sigma_0}{\eta_0\dot{\gamma}_{\rm hex}-\sigma_0}\right)}. \qquad (8)$$

The remaining parameter a' is determined by fitting the numerical results for τ_c/τ at the boundary (see fig. 6) to expression (8), yielding $a'/\tau = 20.62$. The resulting line $\tau_c^{\rm trans}(\dot{\gamma}_{\rm init})$ is included in fig. 6, showing that our estimate describes the transition between quadratic and hexagonal states very well.

Conclusions. – Using numerical simulation we have studied the complex dynamical behaviour of sheared colloidal films under a specific type of shear-stress control. Our approach involves relaxation of the shear rate in a finite relaxation time τ_c, until the instantaneous stress matches its desired value. This approach is inspired by rheological experiments [29] where the instantaneous shear rate as function of time can be measured. Focusing on systems which multivalued flow curves (resulting from successive non-equilibrium transitions) we have found that, by tuning τ_c and the initial conditions, it is possible to *select* a specific dynamical state. In the present system these are either a state with quadratic in-plane ordering and high viscosity, or a hexagonal state with low viscosity. Therefore, our study suggests a way to stabilize states with desired rheological properties, particularly shear viscosities. Moreover, we have proposed a model which relates the transition values of τ_c to relevant *intrinsic* relaxation times under sudden change of $\dot{\gamma}$.

Although most of our results pertain to a colloidal bilayer, the fact that we found analogous results for trilayers indicates that the method is not restricted to thin films alone. Rather, we expect the method to allow for state selection in *any* shear-driven system with multivalued flow

curve. Indeed, in an earlier study we have used an analogous approach (based, however, on continuum equations) to select states and even suppress chaos in shear-driven nematic liquid crystals [27]. It therefore seems safe to assume that the capabilities of the present scheme are quite wide. For colloidal layers one may envision, e.g., stabilisation of *time-dependent structures* such as oscillatory density excitation, which may have profound implications for lubrication properties [39].

Finally, our findings are quite intriguing in the broader context of manipulating nonlinear systems by feedback control. In our case, the feedback character stems from the fact that the stress control involves the configuration-dependent instantaneous stress. Mathematically, this scheme can be viewed as feedback control with exponentially distributed time-delay [40] (as can be seen by formally integrating eq. (3) and inserting it into eq. (1)). Similar schemes are used to stabilize dynamical patterns in laser networks [41], neural systems [43], and more generally, coupled oscillator systems [42]. The implications of these connections are yet to be explored.

* * *

This work was supported by the Deutsche Forschungsgemeinschaft through SFB 910 (project B2).

REFERENCES

[1] M. Ripoll, P. Holmqvist, R. G. Winkler, G. Gompper, J. K. G. Dhont, and M. P. Lettinga, *Phys. Rev. Lett.*, **101** (2008) 168302.
[2] D. Strehober, H. Engel, and S. H. L. Klapp, *Phys. Rev. E*, **88** (2013) 012505.
[3] M. Das, B. Chakrabarti, C. Dasgupta, S. Ramaswamy and A. Sood, *Phys. Rev. E*, **71** (2005) 021707.
[4] P. D. Olmstedt, *Rheol. Acta*, **47** (2008) 283.
[5] R. Moorcroft and S. M. Fielding, *Phys. Rev. Lett*, **110** (2013) 086001.
[6] R. Besseling, L. Isa, P. Ballesta, G. Petekidis, M. E. Cates and W. C. K. Poon, *Phys. Rev. Lett.*, **105** (2010) 268301.
[7] R. L. Moorcroft, M. E. Cates and S. M. Fielding, *Phys. Rev. Lett.*, **106** (2011) 055502.
[8] C.-Y. David Lu, P. D. Olmsted, and R. C. Ball, *Phys. Rev. Lett.*, **84** (2000) 642.
[9] J. Zausch and J. Horbach, *Europhys. Lett.*, **88** (2009) 60001.
[10] P. Chaudhuri and J. Horbach, *Phys. Rev. E*, **88** (2013) 040301.
[11] A. Aradian and M. E. Cates, *Europhys. Lett.*, **70** (2005) 397.
[12] A. Aradian and M. E. Cates, *Phys. Rev. E*, **73** (2006) 041508.
[13] D. Lootens, H. Van Damme, and P. Hebraud, *Phys. Rev. Lett.*, **90** (2003) 178301.
[14] M. E. Cates and S. M. Fielding, *Adv. Phys.*, **55** (2006) 799.
[15] T. H. Besseling, M. Hermes, A. Fortini, M. Dijkstra, A. Imhof and A. van Blaaderen, *Soft Matter*, **8** (2012) 6931.
[16] D. Derks, Y. L. Wu, A. v. Blaaderen and A. Imhof, *Soft Matter*, **5** (2009) 1060.
[17] T. A. Vezirov and S. H. L. Klapp, *Phys. Rev. E*, **88** (2013) 052307.
[18] J. S. Raynaud, P. Moucheront, J. C. Baudez, F. Bertrand, J. P. Guilbaud and P. Coussot, *J. Rheol.*, **46** (2002) 709.
[19] M. E. Cates, S. M. Fielding, D. Marenduzzo, E. Orlandini, and J. M. Yeomans, *Phys. Rev. Lett.*, **101** (2008) 068102.
[20] S. M. Fielding, *Soft Matter*, **3** (2007) 1262.
[21] G. L. Burrell, N. F. Dunlop and F. Separovic, *Soft Matter*, **6** (2010) 2080.
[22] X. Cheng, J. H. McCoy, J. N. Israelachvili and I. Cohen, *Science*, **333** (2011) 6047.
[23] A. Fall, A. Lematre, F. Bertrand, D. Bonn and G. Ovarlez, *Phys. Rev. Lett.*, **105** (2010) 268303.
[24] R. Bandyopadhyay and A. K. Sood, *Europhys. Lett.*, **56** (2001) 447.
[25] F. Frahsa, A. K. Bhattacharjee, J. Horbach, M. Fuchs and T. Voigtmann, *J. Chem. Phys.*, **138** (2013) 12A513.
[26] F. Varnik, L. Bocquet, and J. L. Barrat, *J. Chem. Phys.*, **120** (2004) 2788.
[27] S. H. L. Klapp and S. Hess, *Phys. Rev. E*, **81** (2010) 051711.
[28] V. S. Rudraraju and C. M. Wyandt, *International Journal of Pharmaceutics*, **292** (2005) 53-61.
[29] Y. T. Hu, P. Boltenhagen, and D. J. Pine, *J. Rheol.*, **42** (1998) 1185.
[30] R. Messina and H. Löwen, *Phys. Rev. E*, **73** (2006) 011405.
[31] V. Mansard, A. Colin, P. Chaudhuri, and L. Bocquet, *Soft Matter*, **9** (2013) 7489.
[32] H. J. C. Berendsen, J. P. M. Postma, W. F. van Gunsteren, A. DiNola and J. R. Haak, *J. Chem. Phys.*, **81** (1984) 3684.
[33] S. H. L. Klapp, Y. Zeng, D. Qu and R. von Klitzing, *Phys. Rev. Lett.*, **100** (2008) 118303.
[34] S. Grandner and S. H. L. Klapp, *J. Chem. Phys.*, **129** (2008) 244703.
[35] D. L. Ermak, *J. Chem. Phys.*, **62** (1975) 4189.
[36] B. Lander, U. Seifert, and T. Speck, *J. Chem. Phys.*, **138** (2013) 224907.
[37] S. M. Fielding and P. D. Olmsted, *Phys. Rev. E*, **68** (2003) 036313.
[38] T. Vezirov, S. Gerloff, and S. H. L. Klapp, *to be published.*
[39] A. Vanossi, N. Manini, and E. Tosatti, *PNAS*, **109** (2012) 16429.
[40] P. Hoevel and E. Schöll, *Phys. Rev. E*, **72** (2005) 046203.
[41] T. Juengling, A. Gjurchinovski, and V. Urumov, *Phys. Rev. E*, **86** (2012) 046213.
[42] Y. N. Kyrychko, K. B. Blyuss, and E. Schöll, *Eur. Phys. J. B*, **84** (2011) 307.
[43] Y. Song, Y. Han and Y. Peng, *Neurocomputing*, **121** (2013) 442.